Landscape structures regulate the contrasting response of recession along rainfall amounts

Jun-Yi Lee[1,2], Ci-Jian Yang[2,3], Tsung-Ren Peng[1], Tsung-Yu Lee[4], Jr-Chuan Huang[2]

[1]Department of Soil and Environmental Sciences, National Chung Hsing University, Taichung 402202, Taiwan
[2]Department of Geography, National Taiwan University, Taipei 106319, Taiwan
[3]German Research Centre for Geosciences (GFZ), Telegrafenberg, Potsdam 14473, Germany.
[4]Department of Geography, National Taiwan Normal University, Taipei 106209, Taiwan

Correspondence to: Jr-Chuan Huang(riverhuang@ntu.edu.tw)

Abstract. Streamflow recession reflects hydrological functioning, runoff dynamics, and storage status within catchments. Landscape structures and rainstorms are regarded and hypothesized as drivers of recession response, which is an important consideration for regional water resources management, particularly under climate change. Yet, the documented recession response is inconsistent and diverse. This study tested how landscape structures and rainstorm characteristics regulate the recession response. A total of 291 pairs of recession parameters—the recession coefficient, *a*, and nonlinearity, *b*, from the power-law recession model ($-dQ/dt = aQ^b$)—over 19 subtropical small mountainous rivers with a broad rainfall spectrum were derived using the decorrelation process. The results showed that *a* and *b* respectively increase and decrease with L/G (the ratio of flow-path length to gradient), particularly in small catchments. Additionally, corroborating previous studies, *a* decreased significantly with rainfall amount. However, nonlinearity increases with rainfall amount in larger catchments but decreased in small catchments. This contrasting response, which was contingent upon drainage area and L/G, leads to considerable bias and needs further clarification, particularly for use in assessing regional recession in ungauged catchments under climate change.

1 Introduction

Streamflow recession, the falling segment of a hydrograph, represents the rainfall-runoff process and interactions among different runoffs and aquifers during a rainstorm. Therefore, recession and its associations with runoff paths within the landscape and aquifers, is particularly critical for baseflow estimation (Palmroth et al., 2010). A power-law relationship, $-dQ/dt = âQ^b$, between streamflow declines and streamflow rate Q is widely used to describe recession at the catchment scale (e.g. Brutsaert and Nieber, 1977). The recession coefficient, $â$, approximates the recession rate but is tangled with the unit of streamflow and *b* (see section 2.2.2), which represents the nonlinearity of storage and is the slope of the regression line of dQ/dt vs Q. Since aquifers in various landscape units (e.g., hillslopes, riparian areas, streams, etc.) exhibit different hydraulic properties, landscape structure apparently affects the streamflow recession parameters. In general, parameter $â$ has a positive correlation with drainage density (total stream length/drainage area) and aquifer slope but a negative correlation with aquifer depth, aquifer heterogeneity, and inter-hillslope heterogeneity (e.g., Brutsaert and Nieber, 1977; Rupp and Selker, 2006;

Harman et al., 2009). Parameter b increases with the number of streams (Biswal and Marani, 2010), aquifer heterogeneity (Rupp and Selker, 2006), and inter-hillslope heterogeneity (Harman et al., 2009) and decreases with the total stream length (Biswal and Marani, 2010).

Theoretical works have shown that the streamflow recession parameters are dependent on landscape structure (and thus aquifer conditions) and rainstorms. Rupp and Selker (2006) demonstrated that parameter $\hat{a}$ is negatively correlated with the initial groundwater table (h_0) under unsaturated conditions, while it has a slightly positive correlation under saturated conditions ($h_0 \geq B\tan\phi$, where B is aquifer length and ϕ is the aquifer angle). Harman et al. (2009) used spatial heterogeneity theory to show that a large recharge rate reduces parameter $\hat{a}$, while drainage network theory suggests that parameter $\hat{a}$ is negatively correlated with the streamflow rate (Biswal and Nagesh Kumar, 2014). For parameter b, hydraulic theories indicate that b decreases from 3.0 to 1.5 during the transition from early to late recession as the influence of the upstream boundary condition becomes a factor when the aquifer drains in wet conditions (e.g., Rupp and Selker, 2006). Spatial heterogeneity theory demonstrates that b only slightly increases with a wet antecedent condition (Harman et al., 2009). However, drainage network theory indicates that b increases with storage while the downstream receives more subsurface flow contribution but decreases with storage as the downstream receives less (Biswal and Nagesh Kumar, 2013). The inconsistent responses in $\hat{a}$ and b among theories indicate a complicated interaction between landscape structure and rainstorms during recession, implying that the recession mechanics in different regions need more exploration.

Tables 1 and S1 respectively summarize and compile previous empirical recession studies. There are two main takeaways: 1) The responses of $\hat{a}$ and b to landscape features and structure have been inconsistent. Such inconsistent results might be landscape dependent (e.g. different regional conditions). 2) These inconsistent recession responses might be due to different treatments (e.g. segment extraction, starting point, fitting techniques, etc.). Most previous studies aggregated long-term data (point-cloud) to retrieve representative recession parameters (the centrality of recession), while some recent studies retrieved parameters from individual events to elucidate the temporal variability of recession. Fewer studies simultaneously addressed recession responses to landscape structure and distinct rainstorm events, which are likely dependent on $\hat{a}$ and b in the power law. For example, Biswal and Nagesh Kumar (2013) found that the structure of drainage networks might result in contrasting directions in the response of b to peak flow.

Everything considered, the theory behind recession is still developing, and it is clear that we need a better understanding of how landscape structure and rainstorm characteristics affect streamflow recession, especially with the necessity of regional recession assessments under climate change. Thus, this study derived the recession coefficient and nonlinearity in 19 mountainous catchments across Taiwan with multiyear records of hourly streamflow (291 events in total). These catchments, with drainage areas of 77–2,089 km^2, are characterized by steep, fractured, forested mountains and periodic typhoon invasions. As a result of these characteristics, Taiwan's rivers have short water residence time and limited water retention capacity (Lee et al., 2020). We addressed three research questions: (1) What are the recession characteristics of typhoon events in small mountainous catchments? (2) How do rainfall and landscape variables affect recession parameters in different regions? (3) In what way do landscape variables regulate the response of nonlinearity to rainfall? In this study, we document the spatial

65   patterns of recession parameters in Taiwan (Sect. 3) and then discussed how recession behaviors change in different landscape settings (Sect. 4).

2 Material and methods

2.1 Study area

Taiwan is a mountainous island geographically located at the juncture between the Eurasian and Philippine tectonic plates and
70   climatologically located in the corridor of typhoons. An active mountain belt with frequent typhoons shapes a steep and fractured landscape with verdant forests. The mean annual rainfall is about 2,510 mm, and approx. 40% of annual rainfall is brought by typhoons within a few days. The lowest mean annual temperature is approx. 4°C in montane regions and 22°C in the coastal plains. The mountains of Taiwan reach an elevation of 4,000 m within a short horizontal distance (~75 km) from the coast, creating a steep terrain (Huang et al., 2016). Specifically, the drainage area of most catchments is smaller than ~500
75   km^2, and stream lengths are less than ~55 km. The basic catchment descriptions, including landscape variables, can be found in Table S2. Land cover inventories from the Taiwan Ministry of the Interior (www.moi.gov.tw) were reclassified into three major categories, namely water (C_W), forest (C_F), agriculture (C_A), and others. The landscape metric was retrieved from the digital elevation model with 20m resolution: A is the drainage area [L^2]; DD is the drainage density [L/L^2], defined as the ratio of total stream length to drainage area; S_m is the gradient of the main stem [-]; HI is the hypsometric integral [-]; ELO is the
80   basin elongation [-], defined as the ratio of the diameter of the circle with the same area as the basin to basin length. The flow path is defined as the hillslope grid point following the surface flow direction toward the channel. Flow-path length (L) is the length of this path, flow-path height (H) is the height difference along this path, and G is the flow-path gradient [-]. These flow-path metrics and the L/G ratio, as proxies for the interaction between landscape and climate (Seybold et al., 2017), are often used in the studies of water residence time (e.g., McGuire et al., 2005)
85   Streamflow in this steep mountainous island descends quickly after a typhoon invasion. Thus, hourly streamflow records are required to describe the entire streamflow recession since it only lasts a few days after the peak. This study collected hourly streamflow records during 1986-2014 from the Taiwan Water Resource Agency (www.wra.gov.tw) and Tai-Power Company (www.taipower.com.tw). Only the catchments without large water division infrastructures in the upstream area and with total rainfall greater than 30 mm were used to avoid human-manipulated streamflow data. Based on these criteria, nineteen
90   catchments and 291 events were included for further recession analysis. Commensurate with the hourly streamflow, the hourly rainfall dataset from the Taiwan Central Weather Bureau (www.cwb.gov.tw) was collected, and the Thiessen weighted method was used to estimate areal rainfall in the corresponding catchments. The rainfall period was defined as the elapsed time from 6 h before the rising flow to the peak flow. Hydroclimate metrics of rainstorm and streamflow, including total event rainfall, duration, average and maximum rainfall intensity, total streamflow, peak flow, and antecedent flow, were extracted from these
95   datasets (Table S3).

2.2 Recession analysis

The storage-outflow relationship is typically described by a power law if treating the catchment as a black box. The representative storage is, in fact, composed of many aquifers and thus exhibits a non-linear relationship:

$$Q = mS^n$$

100   (1)

where S is the storage volume within a catchment (in units of volume [L^3] or depth [L]), Q is the rate of streamflow ([L^3/T] or [L/T]), and m and n are constants (Vogel and Kroll, 1992). Since S is difficult to directly measure, the relationship between the rate of streamflow decline and streamflow could be derived to represent the recession behavior (Brutsaert and Nieber, 1977) in Eq. (2).

105    $-\frac{dQ}{dt} = nm^{\frac{1}{n}}Q^{\frac{2n-1}{n}} = \hat{a}Q^b$

(2)

where $\hat{a}$ is the recession rate and b represents the nonlinearity of storage, which is also the slope of the regression line in the plot of dQ/dt vs Q (the recession plot). Both parameters can be estimated via different assumptions and fitting techniques. Notably, since nonlinearity is dimensionless, $\hat{a}$ is inherently strongly dependent on the unit of Q and b via fitting (see details

110 in section 2.2.2). Although the recession plot enables the analysis of streamflow recession and facilitates the derivation of the storage–outflow relationship (Stölzle et al., 2013), the methods of recession segment extraction manipulate parameter estimation. For example, Stölzle et al. (2013) compared three extraction methods in conjunction with their corresponding parameter estimations. They found that recession characteristics, like recession time ($1/\hat{a}$), varied over 1–2 orders of magnitude, yet nonlinearity, b, varied rather narrowly. Their results suggested that the recession characteristics derived from different

115 procedures have only limited comparability. Further, Dralle et al. (2017) found that the relationship between $\hat{a}$ and antecedent wetness was sensitive to the number of data points and thus the extraction method. Despite the estimated parameters being inconsistent among the procedures, applying the same procedure is still a feasible way to capture the recession responses in a region.

2.2.1 Recession segment extraction

120 In the extraction procedure, two concerns should be addressed: (1) distinguishing between the early and late recession stages, and (2) eliminating any unexpectedly positive increases in the recession. The early stage (containing pre-storm and surface flow) and the late stage of recession (dominated only by base flow) are indistinguishable and usually determined subjectively. Some studies have empirically excluded the early-stage recession to eliminate the influence of quick flow (e.g., Brutsaert, 2008; Vogel and Kroll, 1992). Others used a threshold for the minimum length of extraction procedures, which ranged from 2

125 to 10 days (e.g., Mendoza et al., 2003; Vogel and Kroll, 1992). For eliminating unexpected positive increases during recession, several approaches have been proposed as well, for example, smoothing the hydrograph (Vogel and Kroll, 1992), discarding the segment entirely (Brutsaert, 2008; Kirchner, 2009), and breaking-and-rejoining the recession segments (Millares et al.,

2009). Each strategy has its advantages and disadvantages; smoothing the hydrograph may not completely erase the bulges caused by precipitation and discarding the segment loses parts of recession events. Although breaking-and-rejoining the recession, too, disturbs the original streamflow records, the method which maintains the more complete recession event is preferable here.

For the recession segment extraction, first, the recession evolution caused by rainstorms was a main concern, and thus we selected the whole recession segment from the peak flow of all individual rainstorm. The whole recession segment represents the interactive mixing of quick and base flow. Second, we screened and broke down the hydrograph where abrupt bulges emerged, erased positive streamflow increases, and concatenated the remaining segments. This elimination procedure produces a curve quite similar to the master recession curve on a long-term scale (Millares et al., 2009). Third, data points corresponding to extremely low streamflow ($Q < 0.1$ mm h^{-1}) or recession ($-dQ/dt < 0.01$ mm h^{-2}), being likely affected by the limits of streamflow measurement, were excluded. Forth, rainfall events with an unreasonable ratio of total flow to total rainfall ($Q/P > 1.1$ or $Q/P < 0.1$) were also excluded to guarantee the data quality. Ultimately, a total of 298 rainstorms were selected for further parameter estimation.

2.2.2 Parameter fitting

In recession analysis, several fitting methods have been proposed. One is to fit with the lower envelope of the point-cloud (Brutsaert and Nieber, 1977). Evapotranspiration affects recession, leading to higher values of $-dQ/dt$, and taking the lower envelope can prevent this effect. Another is to fit with the entire point-cloud (Brutsaert, 2005; Vogel and Kroll, 1992) as subsoil heterogeneity may overshadow the evapotranspiration effect in larger or steeper catchments (Brutsaert, 2005). Yet another is to fit with the binned means weighted by the square of the standard error of each binned mean (Kirchner, 2009) because the lower values of $-dQ/dt$ could be affected by the measurement errors in the streamflow observations. Recently, a virtual experiment study (Jachens et al., 2020) suggested fitting with individual recession segments to explore the recession responses to individual rainstorms.

The parameter estimation from the retrieved recession segments was described below. Firstly, we corrected low-flow records: The same low flow levels appear frequently in late recession due to the detection limit of instruments, resulting in a series of zero $-dQ/dt$ values that affect parameter estimation, particularly for b. To reduce this bias, we applied the exponential time step method (Roques et al., 2017) in which the time step of the moving window for calculating $-dQ/dt$ exponentially increases along the recession. This extended sampling period helps avoid the occurrence of zero $-dQ/dt$ values (Roques et al., 2017). Secondly, we used the decorrelation method: Another important concern in recession parameter estimation is the dependence between $\hat{a}$ and b, which blurs the interpretation of parameters (Dralle et al., 2015). The decorrelation method assumes that the observed flow, Q, consists of a scale-free flow $\hat{Q}$ and a constant k ($Q = k\hat{Q}$). Thus, the power law formula can be rewritten as $-dQ/dt = ak^{b-1}\hat{Q}^b$, where a is the scale-free recession coefficient [h^{-1}]. For correcting $\hat{a}$ to a, the observed flow Q was divided by a constant Q_0 (which is ideally equal to $1/k$, see detail in Dralle et al., 2015):

160 $$Q_0 = \exp\left(-\frac{\sum_{i=1}^{N}(b_i - \bar{b})(\log(\hat{a}_i) - \overline{\log(\hat{a}_t)})}{\sum_{i=1}^{N}(b_i - \bar{b})^2}\right)$$

(3)

where $\bar{b}$ and $\overline{\log(\hat{a})}$ is the means of the fitted parameters b {b_1, b_2, …, b_N}and $\log(\hat{a})$ {$\log(\hat{a}_1)$, $\log(\hat{a}_2)$, …, $\log(\hat{a}_N)$}, respectively, across N rainfall events in a given catchment. Although the decorrelation method can reduce the unit effect and dependency on b, Biswal (2021) argued that the dependency of $\hat{a}$ and b can't be fully decoupled, and retrieving parameters

165 from the power law and fixing b is preferable. Obviously, decoupling the dependency of $\hat{a}$ and b in recession is unsolved and challenging and necessitates further study. Nevertheless, after the decorrelation process, the number of catchments with a high correlation between a and b ($R^2 > 0.1$) decreased from 9 to 2, apparently mitigating the unit-effect and dependency of b. Finally, events with low goodness of fit ($R^2 < 0.5$) were discarded. As a result, 291 events and all watersheds, with 5 to 26 events each (Table S3), were included for exploring the landscape and rainstorm effects. Each individual storm event may not necessarily

170 occur in all catchments.

3. Results

3.1. Recession parameters from individual and point-cloud fits

The streamflow recession plots of catchments W9, W5, and W8, as examples, are illustrated in Fig. 2. The three catchments have distinct differences in landscape, particularly in drainage area (A) and the ratio of flow-path length to gradient (L/G).

175 Catchment W9 has a larger A and lower L/G, W5 has a smaller A and lower L/G, and W8 has a smaller A but higher L/G, see Table S2 for catchment details. Median b values, in descending order, were 2.34 in catchment W9, 1.96 in W5, and 1.63 in W8. The point-cloud-derived b values were 1.45 (W9), 1.37 (W5), and 0.88 (W8), showing that point-cloud-derived b values are smaller than median-derived values (Fig. 2c). Notably, the nonlinearity decreases with storm magnitude in W5 and W8 but increases with storm magnitude in W9 (Fig. 2b and 2c). This contrasting response coincided with a difference in drainage area

180 and was relatively consistent across all the catchments. This apparent association is explored further in the Discussion section.

The frequency distributions of the fitted recession coefficients and nonlinearities from all catchments and event records are shown in Figure 3a-b. Coefficient a ranged from 0.003 to 0.273 hr^{-1} with a mean of 0.059 hr^{-1} and median of 0.047 hr^{-1}. The large difference between the median and mean reflects a right-skewed distribution. Nonlinearity, b, ranged from 0.90 to 4.39 with a mean of 1.76 and median of 1.69. The small difference between the median and mean suggests a relatively symmetric

185 distribution. Spatial patterns of recession coefficient and nonlinearity are illustrated in Fig. 3c-d. Generally, larger recession coefficients were seen in the southwestern plain catchments (Fig. 3c), which have higher L/G values. Apart from this, no other distinct pattern can be found in other, more mountainous catchments. Conversely, the plot of recession nonlinearity presents a vague pattern (Fig. 3d), and no simple relationship could be found.

The recession parameters derived from individual segments and aggregated point-cloud data are illustrated in Fig. 4. The

190 variations of recession responses from individual segments fluctuated greatly among catchments. For parameter a, point-cloud-derived values, which aggregate all recession segments in a catchment, are much larger than the coefficients from individual segments. Notably, when the drainage area is larger than 800 km^2 (W19 and larger), the point-cloud-derived coefficients become similar to the third quantile of the distribution of individual segments. For nonlinearity, the values derived from the point-cloud are consistently close to the lower limit of the distribution of the individual segment-derived values and the median

195 and interquartile range of nonlinearity derived from individual segments are irrelative of drainage area. These distinct differences between coefficients and nonlinearities from the two fitting methods make comparison and interpretation difficult. The details of the recession characteristics for each catchment can be found in Table S4.

3.2 Relationships between recession parameters and event/landscape variables

To capture how rainfall forcing affects streamflow recession, correlation analyses were performed. The correlation coefficients

200 between recession parameters and event-associated variables are shown in Fig. 5 and Table 2. The total precipitation (P), duration (D), total streamflow (Q_{tot}), antecedent streamflow (Q_{ant}), and runoff coefficient (Q_{tot}/P) were negatively correlated with the recession coefficient, a. The average precipitation intensity (I_{avg}) and peak flow (Q_p), both of which represent the rainstorm magnitude, were not significantly correlated to a. As for initial event conditions, the 7-day antecedent precipitation, AP_{7day}, defined as the seven-day rainfall amount prior to a rainstorm, was not correlated to a, nor were other AP period lengths

205 (3-, 5-, 14-, and 30-day). Unlike the recession coefficient, which was strongly dependent on the hydrometric variables, nonlinearity, b, was only correlated with two, Q_{ant} and Q_p, with positive and negative correlations, respectively. This indicates that higher antecedent flow could lead to higher nonlinearity and peak flow to lower. Overall, hydrometric forcing moderately controls the coefficient and only slightly affects nonlinearity.

Regarding landscape variables, the average height (H), length (L), and gradient (G) of the flow-path were approx. 120 m,

210 252 m, and 0.47, respectively (Table S2). The mean L/G value for our catchments was approx. 951m. Forest was the dominant landscape type, and the average forest coverage was approx. 67.1%, ranging between 11.8-92.1%. Notably, the catchments in the western plain are characterized by gentle gradients of flow-path, such as catchments W8, W9, W11, W12, W13, and W14. Due to the gentle landscape and higher L/G, agricultural activities are the dominant land cover in those catchments. The details of the landscape variables can be found in Table S2.

215 The correlations of recession parameters against landscape variables are illustrated in Fig. 5 and Table 2. Most landscape variables (H, L, G, L/G, DD, S_m, HI, C_W, C_F, and C_A) are significantly correlated with the coefficient, particularly the flow-path-associated ones (H, L, G, L/G, and DD). Flow-path height (H), length (L), and gradient (G) were negatively correlated to the coefficient, but L/G and DD were positively correlated. Additionally, the coefficient increases as HI and S_m decrease. Looking at land cover, the coefficient increases with C_W (proportion of water body land cover) and C_A (proportion of

220 agriculture land cover) and decreases with C_F (proportion of forest land cover). Greater water-body and/or agricultural land area in a catchment lead to a faster recession, yet greater forested land area can slow recession. Correlations between b and the

landscape variables were generally weaker and of the opposite sign than the correlations seen with a. There were also less significant correlations. In short, most landscape variables are moderately associated with the coefficient and low-to-moderately with nonlinearity. Perhaps, putting all catchments with various landscape features together would obscure the landscape's control in recession.

4. Discussion

4.1 Recession parameters in small mountainous rivers

Notably, the parameters derived from the point-cloud and individual segments exhibit distinct systematic biases (Fig. 4). The larger a and smaller b values derived from the point-cloud than from individual segments could be expected since the flood distribution is right-skewed, representing a large number of small cases with scarce extremes. The point-cloud-derived nonlinearity b could be altered either by the numerous small cases or the scarce extreme cases during fitting. Jachens et al. (2020) indicated that the event properties (variation among inter-event, storm magnitude, and antecedent condition) strongly affect parameter estimation. Since a and b are inherently dependent and while the decorrelation method might be valid for some specific cases (Biswal, 2021), the way (e.g. fixing b) to obtain the a or b of an individual event is still goal-dependent (Sharma and Biswal, 2022). Even so, using the median from individual segments is suggested, compared to the point-cloud derivation (Dralle et al., 2017; Jachens et al., 2020).

The recession coefficients observed in our small mountainous rivers varied across a wide range (from 0.003 to 0.273 hr^{-1}), which is similar to ranges seen in other studies, such as 0.012–0.230 for Swedish catchments (Bogaart et al., 2016) and 0.015–0.171 for watersheds in the USA (Biswal and Marani, 2010). Higher median recession coefficients were found in W8, W11, W12, and W14, which we attributed to the landscape features of shorter and gentler flow paths, i.e., dense drainage networks. By contrast, catchments with longer and steeper flow paths, such as W7 and W15, have lower median recession coefficients. Taken together, these data demonstrate how landscape structure, particularly drainage density and flow-path-associated variables, can affect the recession coefficient. The findings presented in Table 2 corroborate this (discussed more in Sect. 4.2). On the other hand, the median of recession nonlinearity, b, is approx. 1.69 (Fig. 3b) with a range of 0.90 to 4.39, also comparable to the ranges found in the literature. For example, values of b from 0.5 to 2.1 could be found in 220 Swedish catchments with low-flow data (Bogaart et al., 2016), 0.6 to 1.7 for 22 Taiwanese rivers derived from low-flow data (Yeh and Huang, 2019), and 1.5 to 3.2 for 67 USA watersheds with event data (Biswal and Marani, 2010). Non-linear storage-outflow relationships (b is not equal to 1.0) are prevalent for most catchments worldwide. In our cases, the highest and lowest median values of b were found in W7 and W19, respectively. Despite the fact that these two catchments have similar landscape structures, their recession nonlinearity exhibits distinct differences. Perhaps, other controlling factors, such as geological structure (i.e., connectivity between the deep aquifer and the stream, heterogeneous hydraulic properties, and/or the interface slope between the shallow and bedrock layers, see Roques et al., 2022) or land cover (Tague and Grant, 2004), might alter recession behavior as well.

4.2 Landscape structure controls on the median of recession parameters

255 Landscape structure aggregates catchment hydraulic properties, embodying recession parameters conceptually. Therefore, recession behaviors in a catchment could be interpreted from two perspectives, hillslope hydraulics and inter-hillslope heterogeneity (Harman et al., 2009), both of which could be represented by the flow-path-associated variables (e.g., H, L, G, L/G, and DD in Table 2) and drainage area. Notably, heterogeneity may increase with drainage area because of the possibility of including a wider range of subsurface conditions. Recession nonlinearity might also increase with drainage area because a

260 larger area accommodates more possibility of superimposition of multiple linear reservoirs, which has been seen in the 68 km2 Mahurangi watershed, New Zealand (McMillan et al., 2014), and the 41 ha Panola Mountain Research Watershed, USA (Clark et al., 2009; Harman et al., 2009), though this does not appear to be the case in our study (Fig. 6a).

The correlation analysis showed that flow-path-associated variables (H, L, G, L/G, DD) only have a vague correlation with the recession nonlinearity (Table 2). This could have two explanations: First, some of our catchments are much larger than

265 500 km^2, which far exceeds the extent of common rainstorms (usually less than 200 km^2). In these large catchments, the limited extent of rainstorms would not bring about a comprehensive recession response in the outflow hydrograph (Huang et al., 2012). Second, the drainage area cannot reflect the unknown number of aquifers (Ajami et al., 2011). Moreover, Karlsen et al. (2019) argued that the dependence of b on landscape variables would change with the streamflow rate. Specifically, flow-path height, H, dominates the nonlinearity during high flow, whereas the drainage area, A, gains more importance during low flow. The

270 relationship between flow-path-associated variables and drainage area and recession needs to be examined in our catchments.

4.2.1 Landscape structure controls on recession coefficient a

Since different combinations of landscape structure and rainstorm characteristics might result in diverse recession responses and drainage area could not solely explain our recession behaviors (Fig. 6a), the flow-path-associated variables and drainage area were used to classify the catchments. Surprisingly, an inverse relationship between the L/G ratio and drainage area

275 emerged (Fig. 6b). The L/G ratio, a measure of the distribution of flow-path length over gradient at a catchment scale, is highly correlated to DD and the topographic wetness index (Beven and Kirkby, 1979). Therefore, L/G is apt to represent the hillslope hydraulics at a catchment scale. In Fig. 6b, all catchments could be simply classified into three types: type A are large catchments (area > 500 km^2), B are small catchments with low L/G, and C are small catchments with high L/G. Another correlation analysis was performed between these parameters and the flow-path-associated variables (H, L, L/G, and DD)

280 according to these classifications (Fig. 7). The recession coefficients correlated with the flow-path-associated variables in small catchments (Type B and C only) significantly. Flow-path height, H, is directly linked to the water table depth in the homogeneous hillslopes. A steeper hillslope corresponds to permeable soils with higher H, leading to a deeper and longer groundwater flow system and slower drainage (Karlsen et al., 2019). High DD and short L lead to a higher recession coefficient due to shorter flow paths. Additionally, McGuire et al. (2005) used isotopic evidence to demonstrate that the residence time

285 increases with L in Oregon, USA. In our case, both DD and L/G (Fig. 7a-c) confirm these documented relations. Small

catchments with a denser stream network (high *DD*) and/or short-and-gentle hillslopes (high *L/G*), have a higher recession coefficient.

4.2.2 Landscape structure controls on recession nonlinearity *b*

The recession nonlinearity conditionally responds to landscape structure (Fig. 7e-7h). If Type A catchments (large area with
290 low *L/G*, gray solid dots in Fig. 7) are excluded, all flow-path-associated variables become significantly correlated with nonlinearity. The positive relationship of *b* with *H* indicates that steeper and rougher hillslopes present non-linear recession behavior. Perhaps with the increase of flow-path length *L*, subsurface runoff has more chances of flowing through various blocks (e.g., temporarily perched groundwater). The two composite indices, *DD* and *L/G*, are negatively related to the value of *b* (Fig. 7g-h). Short-and-gentle hillslopes lead to a larger saturation area (Bogaart et al., 2016; Sayama et al., 2011), and the
295 expansion of the saturation area indicates that the whole subsurface becomes saturated and connected well, thus reducing heterogeneity. It suggested that the *L/G* ratio affects the nonlinearity significantly for small catchments; however, it is not the cases of our large catchments, which necessitates further interpretation associated with scale.

4.3 Rainfall amount controls on the variation of recession parameters

Recession behavior is a convolutional response starting as rain falls within catchments. Thus, we separately examined the
300 recession parameters against hydrometric variables for the three catchment types (Types A, B, and C) to rule out the influences (Fig. 8). This produced two significant findings: (1) the recession coefficient, *a*, decreases with the rainfall amount in all types and (2) the recession nonlinearity, *b*, shows contrasting responses in Type A and B (Type C is statistically insignificant). In heterogeneity-dominated (large) or hydraulics-dominated (small and steep) catchments, *b* increases or decreases with rainfall amount, respectively.

305 ### 4.3.1 Rainfall amount controls on recession coefficient *a*

Several empirical studies found a positive or independent relationship between *a* and streamflow; for example, Santos et al. (2019) found that higher streamflow produced a greater *a* value, reflecting a quick recession in Switzerland's catchments. In Sweden, annual rainfall variation might be independent of the *a* (Bogaart et al., 2016). However, most studies found a negative relationship between *a* and storage measures (Table 1). For instance, Biswal and Nagesh Kumar (2014) found a negative
310 correlation between *a* and the antecedent flow rate, while Ghosh et al. (2015) found that high peak flow events tend to produce a small value of *a*. In our study of three catchment types, recession coefficients decreased with rainfall amount in all catchment types (Fig. 8a-c). Harman et al. (2009) demonstrated that the recession coefficient can be expressed as $a = V_0/R^{b-1}$ (where V_0 and R represent the mean of the velocity distribution of hillslope flow and rainfall rate, respectively). In the case of heavy rainfall, the increase of R is much larger than that of V_0. The effect of this disproportionate rainfall input increase on *a* could
315 offset the increase in flow velocity, resulting in a negative correlation. Moreover, Biswal and Nagesh Kumar (2014) used a geomorphological recession flow model $a \propto c/q^{b-1}$ (where *c* and *q* represent the celerity and rate of channel flow, respectively,

and which is similar to Harman's theory) to explain why "a" is negatively correlated with "q." To sum up, the negative correlation between coefficient a and rainfall amount (e.g. peak flow and prior soil moisture) is consistent with the literature and is prevalently in most regions (also see Table 1).

4.3.2 Opposing controls of rainfall on recession nonlinearity b

Literature covering the variation of recession nonlinearity among events is divergent. Some studies concluded that nonlinearity, b, is controlled by landscape structure and is static or insensitive to rainfall (Biswal and Marani, 2010; Brutsaert and Nieber, 1977; Dralle et al., 2017). In other studies, nonlinearity, b, decreases with streamflow rate, albeit on different temporal scales (Shaw and Riha, 2012; Karlsen et al., 2019; Santos et al., 2019). Some studies have even argued that nonlinearity can change over the course of an event dynamically (Rupp and Selker, 2006; Luo et al., 2018; Roques et al., 2022). In our study, nonlinearity b showed a positive, negative, and flat relationship with rainfall in Type A, B, and C catchments, respectively (Fig. 8d-f). Small catchment areas (Type B and C catchments) may be explained by a 2-dimensional hillslope model (Roques et al., 2022). During heavy rainfall, when fast flow pathways are activated, the nonlinearity of recession would decrease. Type B catchments (Steep slopes) with more heterogeneous hydraulic conductivity would experience larger changes in recession nonlinearity, whereas Type C catchments (gentle slopes) with more homogeneous hydraulic conductivity would experience smaller changes in recession nonlinearity. Conversely, the nonlinearity, b, increases with the rainfall amount in Type A catchments. In large and heterogeneous catchments, the expansion of the contributing area is less steady and more complicated, and thus the nonlinearity increases with rainfall amount. A contrasting response of b to rainfall similar to the one seen in this study was also found in Biswal and Nagesh Kumar (2013), which attributed it to the change in subsurface flow contributions along the channel that affect the response direction of b. Our study revealed that landscape structure and rainfall amount control the direction and magnitude of recession response, respectively. Future research could further consider different landscape structures when modeling the intra-event variation of b.

4.4 Landscape structure regulates recession behavior

The above two sections have demonstrated the influence of landscape and rainfall amount on streamflow recession behavior. Thus, a perceptual model which demonstrates the interactive regulation of landscape structure and rainfall amount on recession nonlinearity is introduced (Fig. 9). Landscape structure is considered in two contexts, spatial heterogeneity (drainage area) and hillslope hydraulics (L/G). The drainage area may correlate to the number of perched storages within the catchments, and the L/G ratio, encapsulating hillslope geometry, can indicate the dynamics of the contributing area associated with runoff generation. Along the spatial heterogeneity dimension (from Type B to A, with increasing drainage area), additional perched storages respond increasingly with rainfall amount and thus enhance the recession nonlinearity. Perched storages are expected to occur where the hydrological conductivity abruptly decreases due to heterogeneous soil properties or geological structures. The existence of perched storages was found in an experimental forested catchment in Taiwan through an intensive soil water monitoring scheme (Liang, 2020). Large catchments may suffer uneven spatial rainfall, which activates perched storages

locally, and thus, the nonlinearity increases. On the other hand, along the L/G dimension (increasing from Type B to C), the heterogeneities of hydraulic conductivities decrease. Heavy rainfall, causing saturation and expansion of the saturation area, can mediate the heterogeneity of hydraulic conductivity and thereby reduce nonlinearity.

5. Summary

Streamflow recession, which reflects the rainfall-runoff process after rainstorms, is crucial for baseflow assessment. This study investigated the effects of landscape structure and rainfall amount on recession using power-law recession analysis for 291 rainfall events in small mountainous rivers. Despite the power-law equation being widely used, different procedures of segment extraction, starting point selection, selection of the point-cloud or individual segment fitting method, fitting details, and so on usually result in considerably disparate and inconsistent parameter estimations. This implies that it is not possible to infer recession characteristics by comparing the parameters found in the literature. The coefficient and nonlinearity derived from point-cloud are considerably larger and smaller, respectively, than the median of individual segments.

In our cases, landscape structure is moderately correlated to coefficient, but only modestly to nonlinearity. If classifying the catchments in accordance with spatial heterogeneity (drainage area) and hillslope hydraulics (L/G), the coefficient increases with L/G and nonlinearity decreases with L/G significantly in small catchments. This likely reveals that both spatial heterogeneity and hydraulic properties regulate recession simultaneously. Along the hillslope hydraulics dimension, small catchments with high L/G attributed to their short-and-gentle hillslopes, have higher recession coefficients. Additionally, L/G is negatively correlated to nonlinearity for small catchments, perhaps because short-and-gentle hillslopes can expand saturation area and connect different aquifers easily, thus reducing nonlinearity. Note that a and b are inherently dependent, so some uncertainty might be involved. Even so, both parameters, whether derived using the point-cloud or individual segments (Fig. 4), present similar fluctuations among catchments, which supports our arguments.

Further, rainfall amount also plays a dominant role in estimating parameter a. It decreases with rainfall amount for all catchments. On the other hand, contrasting response directions of nonlinearity to rainfall amount could be found along the dimension of spatial heterogeneity (drainage area). Larger catchments exhibited an increase in recession nonlinearity with higher rainfall, whereas smaller catchments showed a decrease in recession nonlinearity with higher rainfall. Conjointly, an interactive regulation of recession by landscape structure and rainfall amount was proposed. In sum, landscape structure (spatial heterogeneity and hillslope hydraulics) may determine the recession behavior via various aquifer settings, and the rainfall amount tunes the magnitude of recession nonlinearity. If the perceptual model is valid, two challenges should be addressed further. First, the contrasting response direction of nonlinearity to rainfall, depending on the predominance of spatial heterogeneity, requires further theoretical validation. Clarifying which environmental factors could represent the spatial heterogeneity and hillslope hydraulics is also an arduous task but is crucial for recession estimation. Second, the careful determination of the response direction of nonlinearity is crucial to the regional recession assessment. An incorrect direction

380 would strongly affect the interpretation, particularly for climatic scenarios. Validating the landscape structure control in rainstorm scale would aid in completing the understating of recession variations.

Data availability. Hourly streamflow data can be obtained from Taiwan Water Resource Agency and Tai-Power company. The authors declare that data supporting the findings of this study are accessible from the article and its supplementary

385   materials.

Author contributions. Conceptualization and Methodology: JYL and JCH. Data Curation and Validation: TYL. Formal analysis: JYL and CJY. Investigation and Writing – Original Draft: JYL. Writing – Review and Editing: JCH and TRP.

390   *Competing interests.* The authors claim no potential competing interests

Acknowledgements. This research was funded by the Ministry of Science and Technology, Taiwan (110-2811-M-005-509, and 109-2811-B-002-631) and the NTU Research Center for Future Earth (107L901004). J. Y. Lee and C. J. Yang was supported by the grants from Ministry of Science and Technology, Taiwan (110-2811-M-005-521, 110-2917-I-564-009).

395

References

Ajami, H., Troch, P. A., Maddock III, T., Meixner, T., and Eastoe, C.: Quantifying mountain block recharge by means of catchment-scale storage-discharge relationships, Water Resour. Res., 47, W04504, https://doi.org/10.1029/2010WR009598, 2011.

400 Beven, K. J. and Kirkby, M. J.: A physically based, variable contributing area model of basin hydrology, Hydrol. Sci. J., 24, 43–69, https://doi.org/10.1080/02626667909491834, 1979.

Biswal, B. and Marani, M.: Geomorphological origin of recession curves, Geophys. Res. Lett., 37, L24403, https://doi.org/10.1029/2010GL045415, 2010.

Biswal, B. and Nagesh Kumar, D.: Study of dynamic behaviour of recession curves, Hydrol. Process., 28, 784–792, 405 https://doi.org/10.1002/hyp.9604, 2014.

Biswal, B., and Nagesh Kumar, D.: A general geomorphological recession flow model for river basins. Water Resour. Res., 49(8), 4900-4906, https://doi.org/10.1002/wrcr.20379, 2013.

Biswal, B.: Decorrelation is not dissociation: there is no means to entirely decouple the Brutsaert-Nieber parameters in streamflow recession analysis, Adv. Water. Resour., 147, 103822, https://doi.org/10.1016/j.advwatres.2020.103822, 2021.

410 Bogaart, P. W., Van Der Velde, Y., Lyon, S. W., and Dekker, S. C.: Streamflow recession patterns can help unravel the role of climate and humans in landscape co-evolution, Hydrol. Earth Syst. Sci., 20, 1413–1432, https://doi.org/10.5194/hess-20-1413-2016, 2016.

Brutsaert, W. and Nieber, J. L.: Regionalized drought flow hydrographs from a mature glaciated plateau, Water Resour. Res., 13, 637–643, https://doi.org/10.1029/WR013i003p00637, 1977.

415 Brutsaert, W.: Hydrology: an introduction, Cambridge university press, https://doi.org/10.1017/CBO9780511808470, 2005.

Brutsaert, W.: Long-term groundwater storage trends estimated from streamflow records: Climatic perspective, Water Resour. Res., 44, W02409, https://doi.org/10.1029/2007WR006518, 2008.

Clark, M. P., Rupp, D. E., Woods, R. A., Tromp-van Meerveld, H., Peters, N., and Freer, J.: Consistency between hydrological models and field observations: linking processes at the hillslope scale to hydrological responses at the watershed scale, 420 Hydrol. Process. Int. J., 23, 311–319, https://doi.org/10.1002/hyp.7154, 2009.

Dralle, D. N., Karst, N. J., Charalampous, K., Veenstra, A., and Thompson, S. E.: Event-scale power law recession analysis: quantifying methodological uncertainty, Hydrol. Earth Syst. Sci., 21, 65–81, https://doi.org/10.5194/hess-21-65-2017, 2017.

Dralle, D., Karst, N., and Thompson, S. E.: a, b careful: The challenge of scale invariance for comparative analyses in power law models of the streamflow recession. Geophys. Res. Lett., 42(21), 9285-9293, https://doi.org/10.1002/2015GL066007, 425 2015.

Harman, C. J., Sivapalan, M., and Kumar, P.: Power law catchment-scale recessions arising from heterogeneous linear small-scale dynamics, Water Resour. Res., 45, W09404, https://doi.org/10.1029/2008WR007392, 2009.

Huang, J.-C., Lee, T.-Y., and Lee, J.-Y.: Observed magnified runoff response to rainfall intensification under global warming, Environmental Research Letters, 9, 034008, https://doi.org/10.1088/1748-9326/9/3/034008, 2014.

430 Huang, J.-C., Lee, T.-Y., Lin, T.-C., Hein, T., Lee, L.-C., Shih, Y.-T., Kao, S.-J., Shiah, F.-K., and Lin, N.-H.: Effects of different N sources on riverine DIN export and retention in a subtropical high-standing island, Taiwan, Biogeosciences, 13, 1787–1800, https://doi.org/10.5194/bg-13-1787-2016, 2016.

Huang, J.-C., Yu, C.-K., Lee, J.-Y., Cheng, L.-W., Lee, T.-Y., and Kao, S.-J.: Linking typhoon tracks and spatial rainfall patterns for improving flood lead time predictions over a mesoscale mountainous watershed, Water Resour. Res., 48,

435 W09540, https://doi.org/10.1029/2011WR011508, 2012.

Jachens, E. R., Rupp, D. E., Roques, C., and Selker, J. S.: Recession analysis revisited: impacts of climate on parameter estimation, Hydrol. Earth Syst. Sci., 24, 1159–1170, https://doi.org/10.5194/hess-24-1159-2020, 2020.

Karlsen, R. H., Bishop, K., Grabs, T., Ottosson-Löfvenius, M., Laudon, H., and Seibert, J.: The role of landscape properties, storage and evapotranspiration on variability in streamflow recessions in a boreal catchment, J. Hydrol., 570, 315–328,

440 https://doi.org/10.1016/j.jhydrol.2018.12.065, 2019.

Kirchner, J. W.: Catchments as simple dynamical systems: Catchment characterization, rainfall-runoff modeling, and doing hydrology backward, Water Resour. Res., 45, W02429, https://doi.org/10.1029/2008WR006912, 2009.

Lee, J.-Y., Shih, Y.-T., Lan, C.-Y., Lee, T.-Y., Peng, T.-R., Lee, C.-T., Huang, J.-C.: Rainstorm Magnitude Likely Regulates Event Water Fraction and Its Transit Time in Mesoscale Mountainous Catchments: Implication for Modelling

445 Parameterization. Water, 12, 1169, https://doi.org/10.3390/w12041169, 2020.

Liang, W. L.: Dynamics of pore water pressure at the soil–bedrock interface recorded during a rainfall-induced shallow landslide in a steep natural forested headwater catchment, Taiwan. J. Hydrol., 587, 125003, https://doi.org/10.1016/j.jhydrol.2020.125003, 2020.

Luo, Z., Shen, C., Kong, J., Hua, G., Gao, X., Zhao, Z., Zhao, H., and Li, L.: Effects of unsaturated flow on hillslope recession

450 characteristics. Water Resour. Res., 54(3), 2037-2056, https://doi.org/10.1002/2017WR022257, 2018

McGuire, K., McDonnell, J. J., Weiler, M., Kendall, C., McGlynn, B., Welker, J., and Seibert, J.: The role of topography on catchment-scale water residence time, Water Resour. Res., 41, W05002, https://doi.org/10.1029/2004WR003657, 2005.

McMillan, H., Gueguen, M., Grimon, E., Woods, R., Clark, M., and Rupp, D. E.: Spatial variability of hydrological processes and model structure diagnostics in a 50 km^2 catchment, Hydrol. Process., 28, 4896–4913, https://doi.org/10.1002/hyp.9988,

455 2014.

Mendoza, G. F., Steenhuis, T. S., Walter, M. T., and Parlange, J.-Y.: Estimating basin-wide hydraulic parameters of a semi-arid mountainous watershed by recession-flow analysis, J. Hydrol., 279, 57–69, https://doi.org/10.1016/S0022-1694(03)00174-4, 2003.

Millares, A., Polo, M. J., and Losada, M. A.: The hydrological response of baseflow in fractured mountain areas, Hydrol. Earth

460 Syst. Sci., 13, 1261–1271, https://doi.org/10.5194/hess-13-1261-2009, 2009.

Palmroth, S., Katul, G. G., Hui, D., McCarthy, H. R., Jackson, R. B., and Oren, R.: Estimation of long-term basin scale evapotranspiration from streamflow time series, Water Resour. Res., 46, W10512, https://doi.org/10.1029/2009WR008838, 2010.

Roques, C., Rupp, D. E., and Selker, J. S.: Improved streamflow recession parameter estimation with attention to calculation
465   of− dQ/dt. Adv. Water Resour.   , 108, 29-43, https://doi.org/10.1016/j.advwatres.2017.07.013, 2017

Rupp, D. E., and Selker, J. S.: On the use of the Boussinesq equation for interpreting recession hydrographs from sloping aquifers. Water Resour. Res., 42(12), https://doi.org/10.1029/2006WR005080, 2006.

Santos, A. C., Portela, M. M., Rinaldo, A., and Schaefli, B.: Estimation of streamflow recession parameters: New insights from an analytic streamflow distribution model, Hydrol. Process., 33, 1595–1609, https://doi.org/10.1002/hyp.13425, 2019.

470   Sayama, T., McDonnell, J. J., Dhakal, A., and Sullivan, K.: How much water can a watershed store?, Hydrol. Process., 25, 3899–3908, https://doi.org/10.1002/hyp.8288, 2011.

Seybold, H., Rothman, D. H., and Kirchner, J. W.: Climate's watermark in the geometry of stream networks. Geophysical Research Letters, 44(5), 2272-2280, https://doi.org/10.1002/2016GL072089, 2017.

Shaw, S. B. and Riha, S. J.: Examining individual recession events instead of a data cloud: Using a modified interpretation of
475   dQ/dt–Q streamflow recession in glaciated watersheds to better inform models of low flow, J. Hydrol., 434, 46–54, https://doi.org/10.1016/j.jhydrol.2012.02.034, 2012.

Shiu, C., Liu, S. C., Fu, C., Dai, A., and Sun, Y.: How much do precipitation extremes change in a warming climate?, Geophys. Res. Lett., 39, L17707, https://doi.org/10.1029/2012GL052762, 2012.

Stölzle, M., Stahl, K., and Weiler, M.: Are streamflow recession characteristics really characteristic?, Hydrol. Earth Syst. Sci.,
480   17, 817–828, https://doi.org/10.5194/hess-17-817-2013, 2013.

Tague, C. and Grant, G. E.: A geological framework for interpreting the low-flow regimes of Cascade streams, Willamette River Basin, Oregon, Water Resour. Res., 40, W04303, https://doi.org/10.1029/2003WR002629, 2004.

Vogel, R. M. and Kroll, C. N.: Regional geohydrologic-geomorphic relationships for the estimation of low-flow statistics, Water Resour. Res., 28, 2451–2458, https://doi.org/10.1029/92WR01007, 1992.

485   Yeh, H. and Huang, C.: Evaluation of basin storage–discharge sensitivity in Taiwan using low-flow recession analysis, Hydrol. Process., 33, 1434–1447, https://doi.org/10.1002/hyp.13411, 2019.

Table 1: Summary of empirical recession study results. Blue, red, and grey shades represent positive, negative, and no correlation with factors, respectively. Numbers inside cells correspond to the reference numbers in Table S1. The asterisk (*) represents this study.

Factor	Centrality of recession — Long-term â	Long-term b	Inter-annual â	Inter-annual b	Inter-seasonal â	Inter-seasonal b	Inter-event â	Inter-event b
Climate/Moisture								
Rainfall	1, 21	1 / 21	21	21			*	* / * / *
Maximum monthly rainfall		2						
Antecedent flow					4, 5		5, 13, 22, *	*
Peak flow							8, * / 6	19, * / 19, * / 8, *
Flow rate after peak							5, 6, 9 / 23	23
Total storage change						11		
Water table elevation					3	3		
Saturated area					3	3		
60 cm soil moisture					3	3		
Baseflow	1							
Evapotranspiration	1, 21	1 / 21			3, 12, 24	24 / 3		
Aridity index	16, 17, 21	15, 16, 17, 21						
Mean relative humidity		2						
Landscape								
Drainage area	10, 16, 20 / 1, *	1, 7, 16, 18, 24 / 20, *						
Long shape of catchment	10 / *	*						
Flow path height	*	24, *						
Flow path length	*	*						
Flow path gradient	*	*						
Mean elevation		2						
Standard deviation of elevation		2						
Catchment slope	17, 24	2, 17, 24						

Hypsometric integral	*	*			
Coefficient of variation of slope	16	16			
Topographic wetness index		2			
Ratio of flow-path length to gradient	*	*			
Drainage density	14, *	14			
	10	*			
Subsurface flow contact time		2			
Landcover					
Reforestation			21	21	
Water management			21	21	
Plateaus coverage		15			
Young volcano rock coverage	14	14			
Forest coverage	18, *	*			
Water bodies coverage	*	16, 21, 24			
	21				
	16	*			
Flood attenuation due to lakes	1	1			
Soil					
Soil depth		24			
Surface hydraulic conductivity	17	21			
	18	17			
Field capacity	16	16			
Moderate infiltration rate soils		2			
Slow infiltration rate soils		2			
Playas with impermeable soils		15			
Organic matter content		2			

Table 2: Spearman correlation coefficients between logarithmic hydrometric characteristics and recession characteristics for all rainfall events at all catchments (n = 291). Grey shades represent statistically significant at the 99% confidence level (p-value < 0.01).

Variable	Meaning	a [hr^{-1}]	b [-]
Hydrometric			
AP_{7day} [mm]	7-day antecedent precipitation	-0.080	0.010
P [mm]	Total precipitation	-0.524	-0.083
D [hr]	Duration of precipitation	-0.432	-0.054
I_{avg} [mm hr^{-1}]	Averaged precipitation intensity	-0.257	-0.026
Q_{tot} [mm]	Total streamflow	-0.609	-0.154
Q_{ant} [mm]	Antecedent streamflow	-0.339	0.266
Q_p [mm]	Peak flow	-0.247	-0.228
Q_{tot}/P [-]	Runoff coefficient	-0.337	-0.097
Landscape			
H [m]	Flow-path height	-0.491	0.224
L [m]	Flow-path length	-0.520	0.302
G [-]	Flow-path gradient	-0.453	0.189
L/G [m]	Ratio of flow-path length to gradient	0.470	-0.181
A [km^2]	Drainage area	0.040	-0.095
DD [km]	Drainage density	0.420	-0.217
S_m [%]	Gradient of main stem	-0.318	0.229
HI [-]	Hypsometric integral	-0.498	0.226
ELO [-]	Basin elongation	-0.209	0.319
C_W [%]	Land cover - water bodies	0.330	-0.147
C_F [%]	Land cover - forest	-0.281	0.140
C_A [%]	Land cover - agriculture	0.268	-0.059
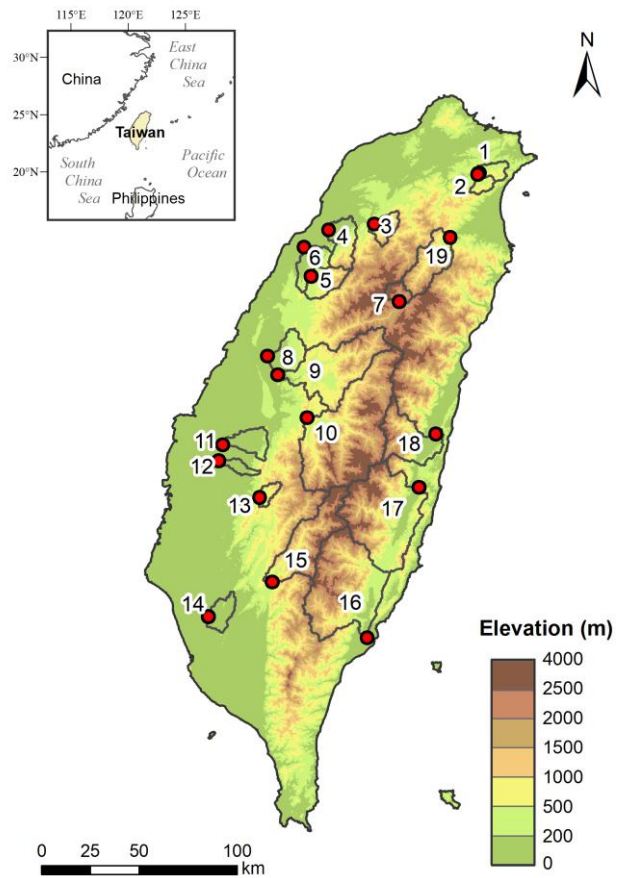
500

Figure 1: Topographic map of Taiwan and the locations of the selected catchments (red dots) and associated watersheds (outlines). The catchment IDs correspond to the IDs in Tables S2 and S3, in which the primary descriptions of hydrologic events and landscape variables are listed.

505
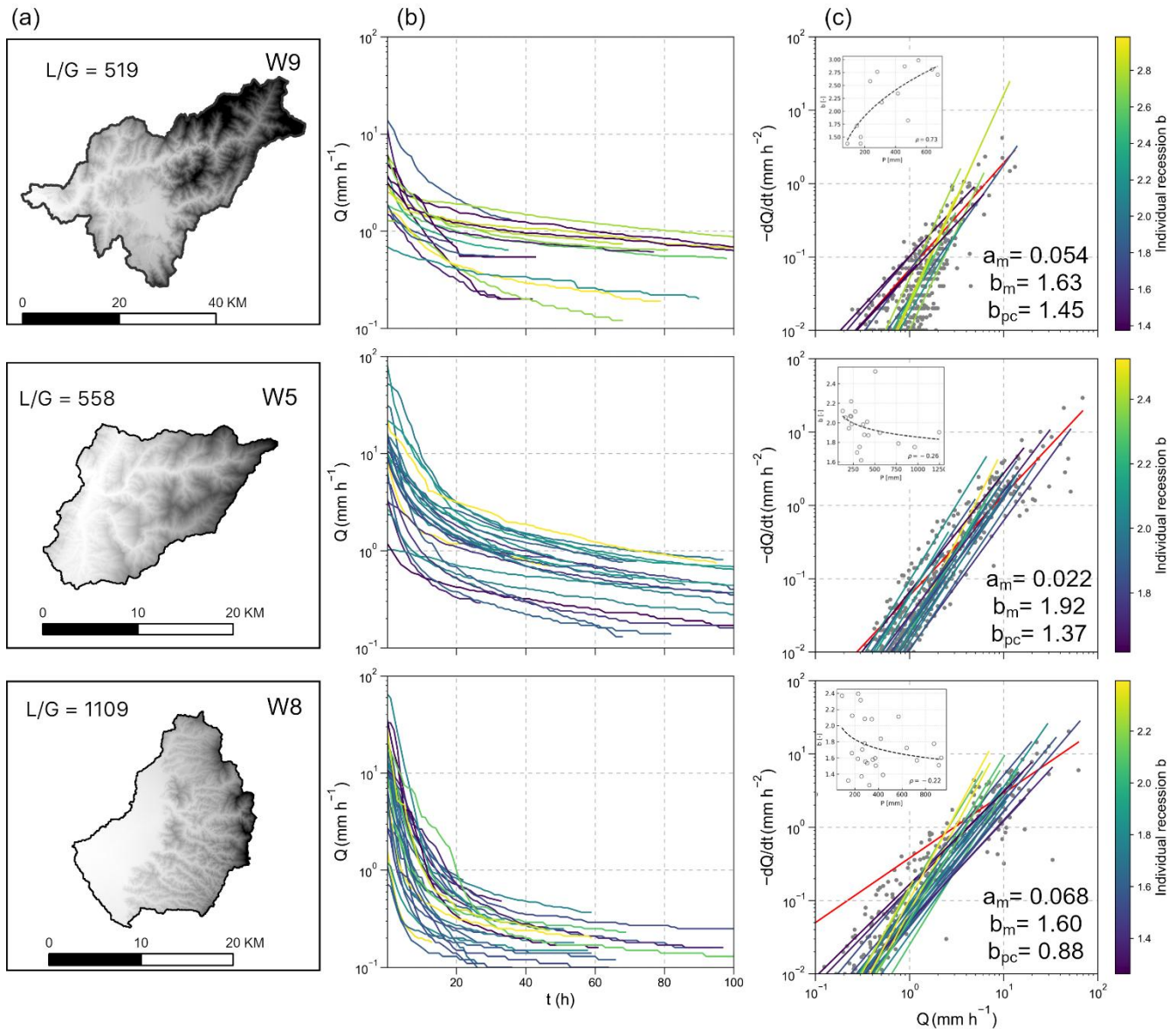
Figure 2: Landscape and recession plots for catchment W9 (row 1), W5 (row 2), and W8 (row 3). Landscape and flow-path topography (L/G) are shown in column (a). Selected recession segments from different rainstorms are shown in (b). Recession plots of all selected rainstorms are shown in column (c). The median of recession parameters *a* and *b$_m$*
and the parameter *b$_{pc}$* derived from the point-cloud are shown in the lower-right corner. The recession *b* from individual segments are colored from purple to yellow with increasing value of *b*, and the red line represents *b* derived using the point-cloud method.

510
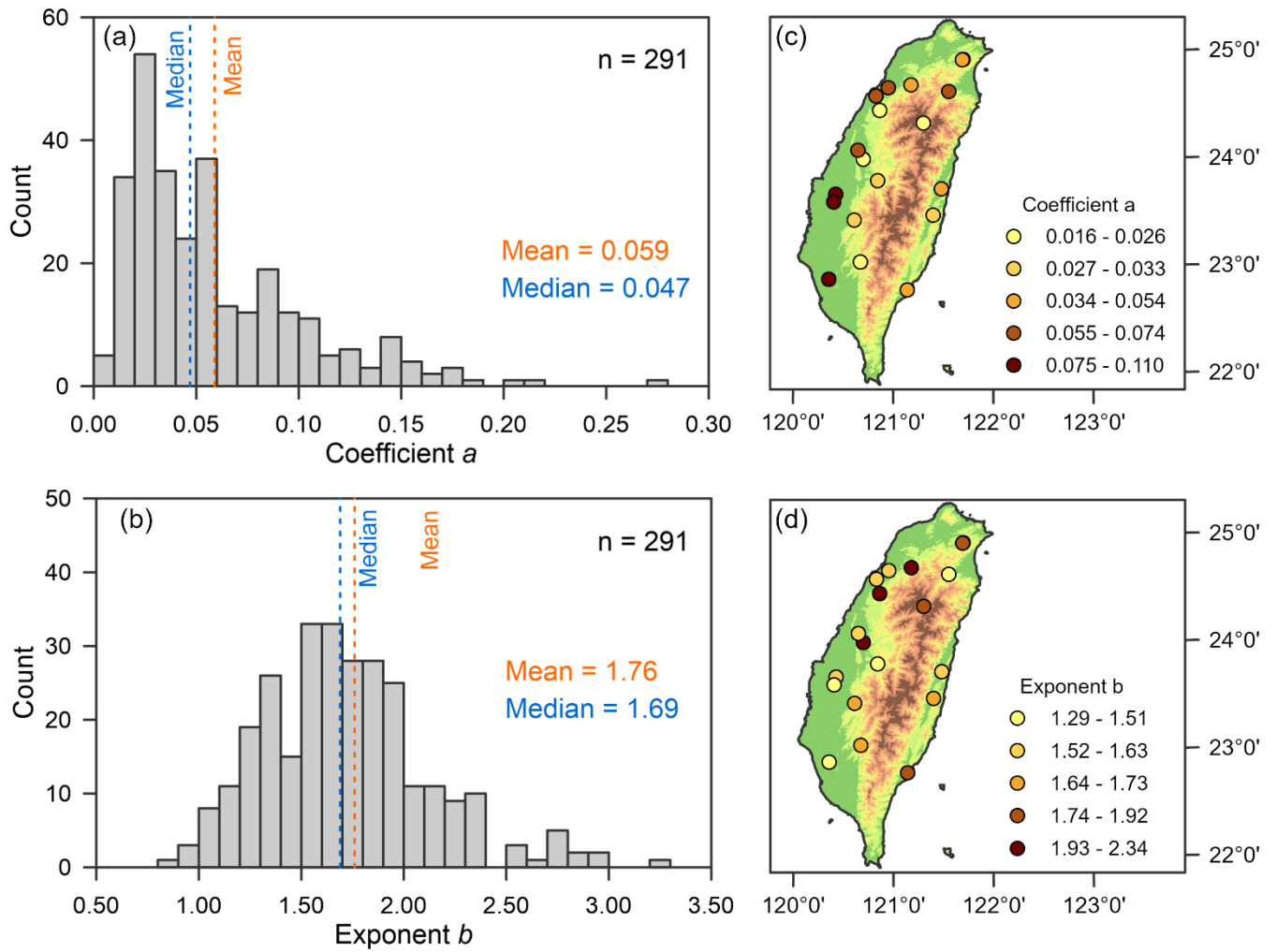
Figure 3: Distributions of recession parameters *a* (a) and *b* (b) estimates in all catchments and events. The spatial distributions of the medians of parameters *a* (c) and *b* (d). The colors of the dots represent the quantiles category.
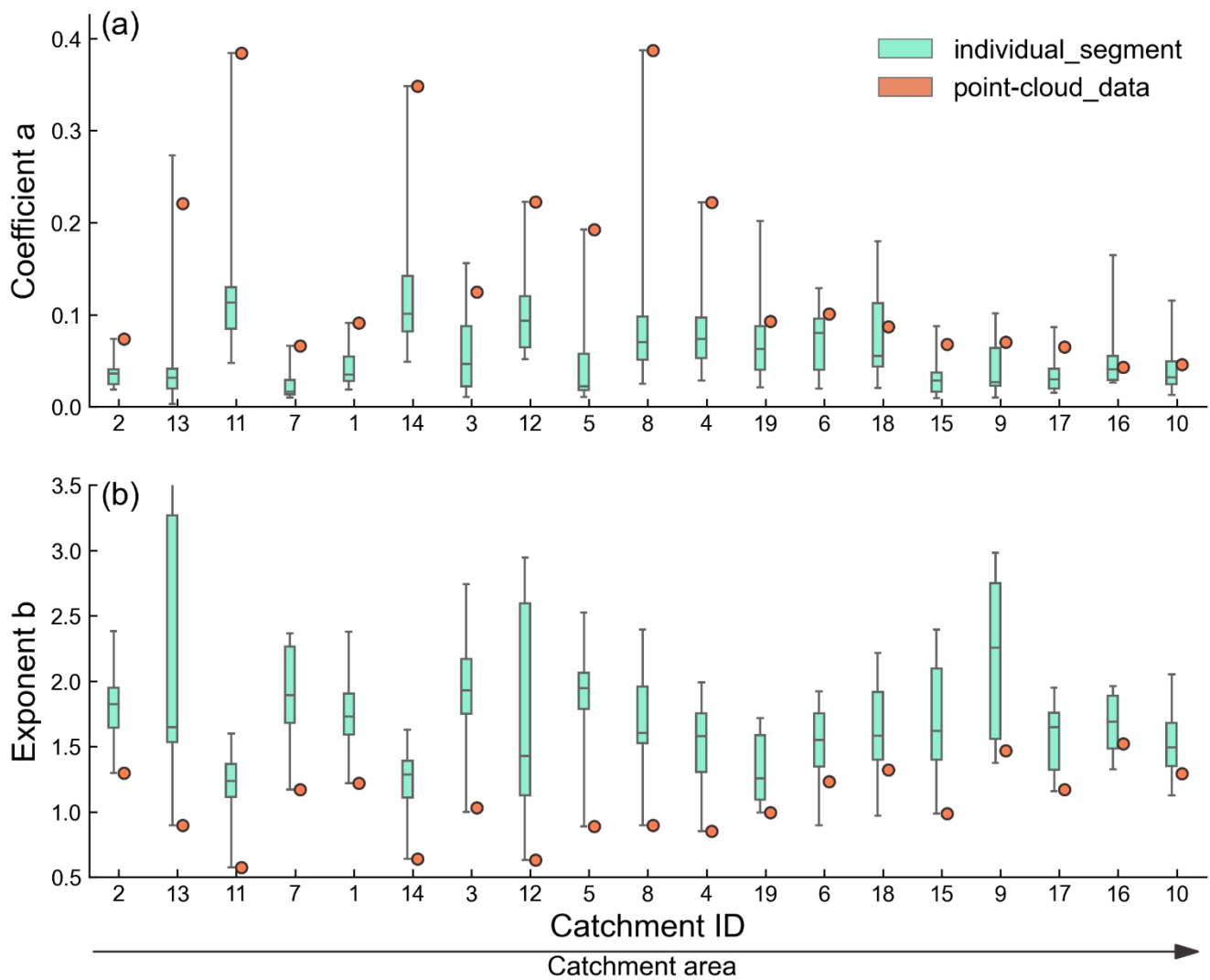
Figure 4: Boxplots of coefficient *a* (a) and exponent *b* (b) derived from the individual recession segments (cyan box) and point-cloud data (orange dot). The catchments are arranged on the *x*-axis in ascending order according to drainage area. Boxes show the interquartile and data range.
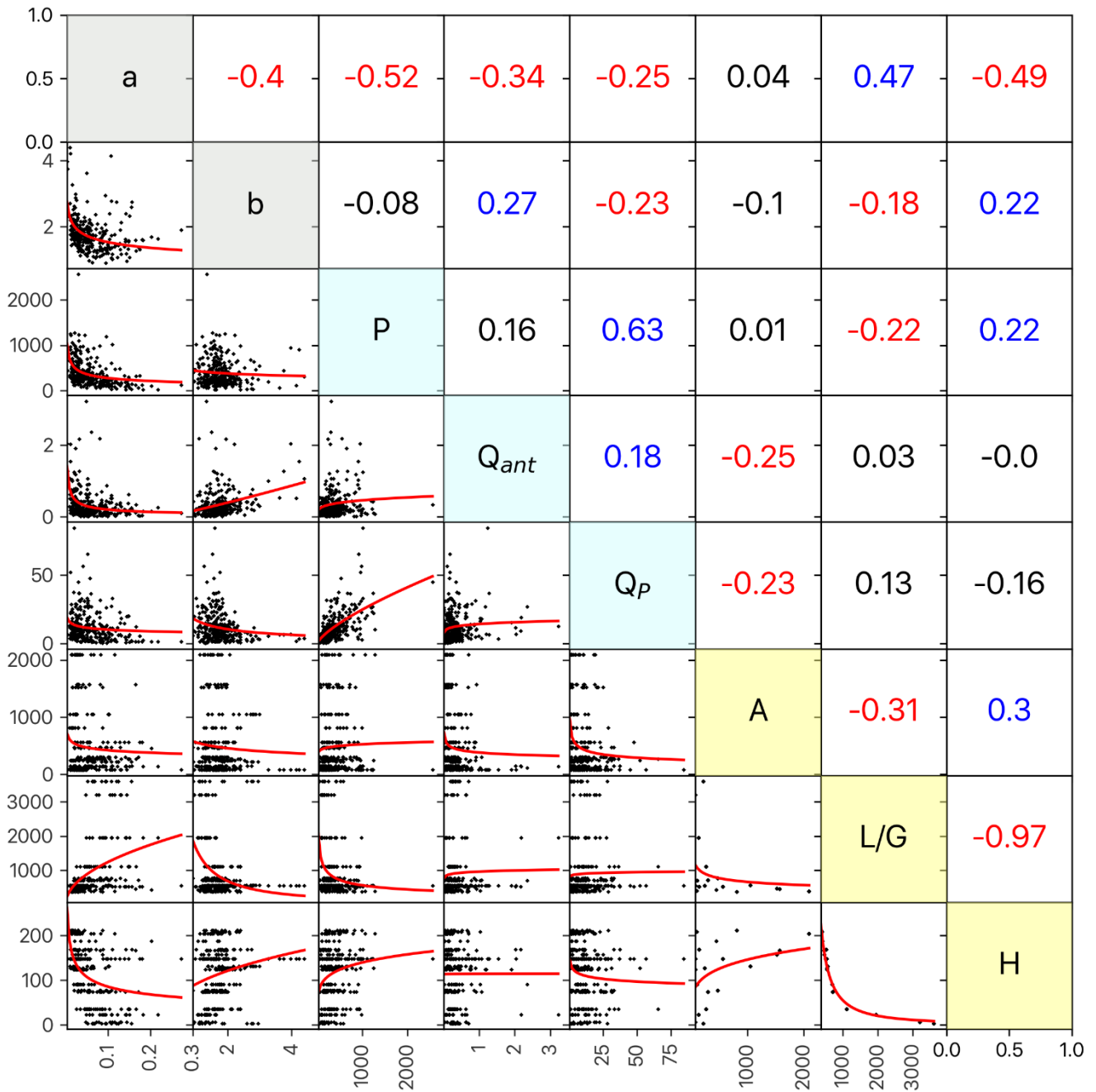
525 **Figure 5: Correlation of recession parameters *a* and *b* against rainstorm event and landscape variables. Below the diagonal: pairwise scatter plots of the recession parameters and variables with a power-fit regression (red line). Above the diagonal: corresponding Spearman correlation coefficients. Blue and red values indicate statistically significant (*p* < 0.05) positive and negative correlations, respectively. Note that all catchments and events are shown in this figure.**
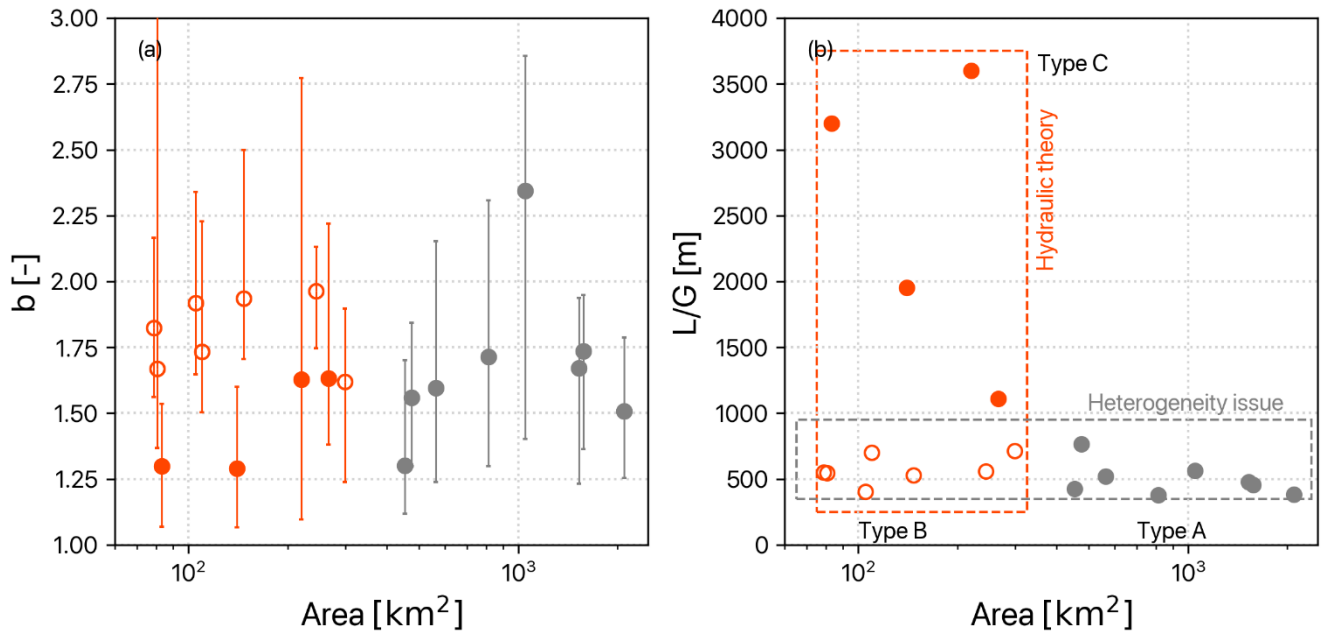
530

Figure 6: The relationship between drainage area and the recession exponent *b* (a) and the flow path topography (*L/G*) (b). The error bar on (a) is the range of the individual segment recession exponent values of each catchment. The orange and gray dots represent small and large catchments (< and > 500 km², respectively), respectively, and the solid and hollow dots represent large and small L/G. The recession behaviors in small and large catchments could be explained
535 **from two perspectives: hydraulic theory (orange box) and heterogeneity issues (gray box).**
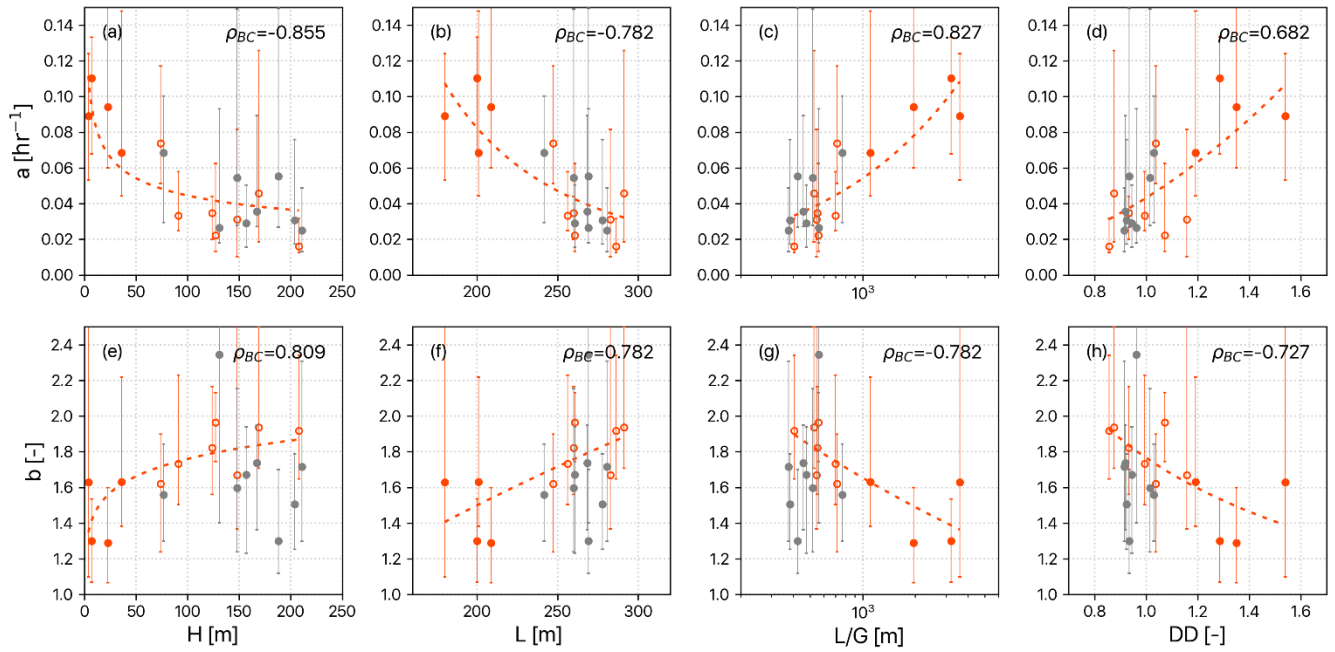
Figure 7: Scatter plots of the median and the range of 10th-90th percentile of recession parameters at each catchment against landscape variables. Gray solid, orange hollow, and orange solid dots are Type A, B, and C basins, respectively. The orange dash line is the power-law fit for small catchments (Type B and C). The Spearman correlation coefficient (ρ) is listed in the upper-right corner of each panel.
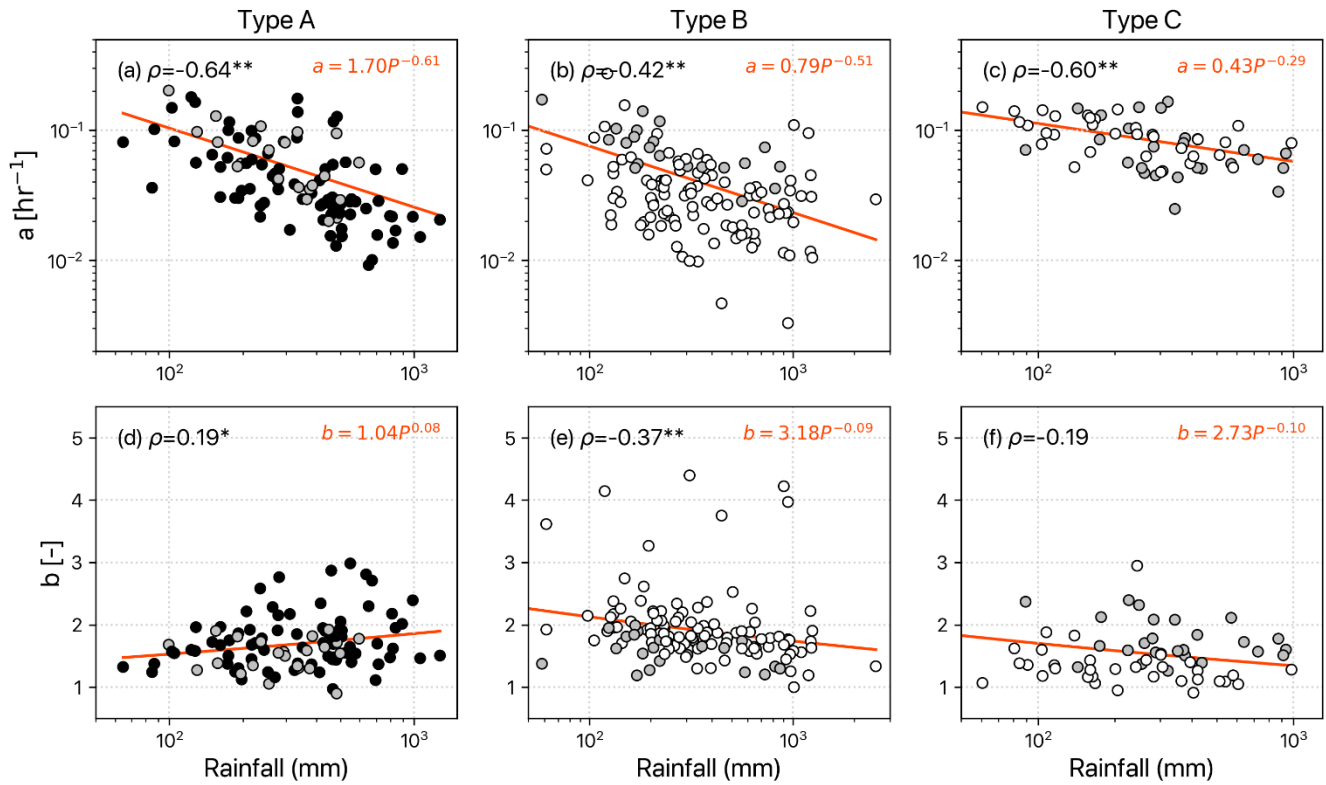
545

Figure 8: Scatter plots of recession parameters against total rainfall for recession segments at different catchment types. Type A are large catchments (area > 500 km^2), B are small catchments with low *L/G* ratios, and C are small catchments with high *L/G* ratios. Black, gray, and white dot colors represent the low, medium, and large L/G catchments, respectively. The orange line is the power-law fit curve with Spearman correlation coefficients in the upper-left corner

550 **of each panel (* and ** denote statistical significance at the 90% and 99% level of confidence, respectively).**
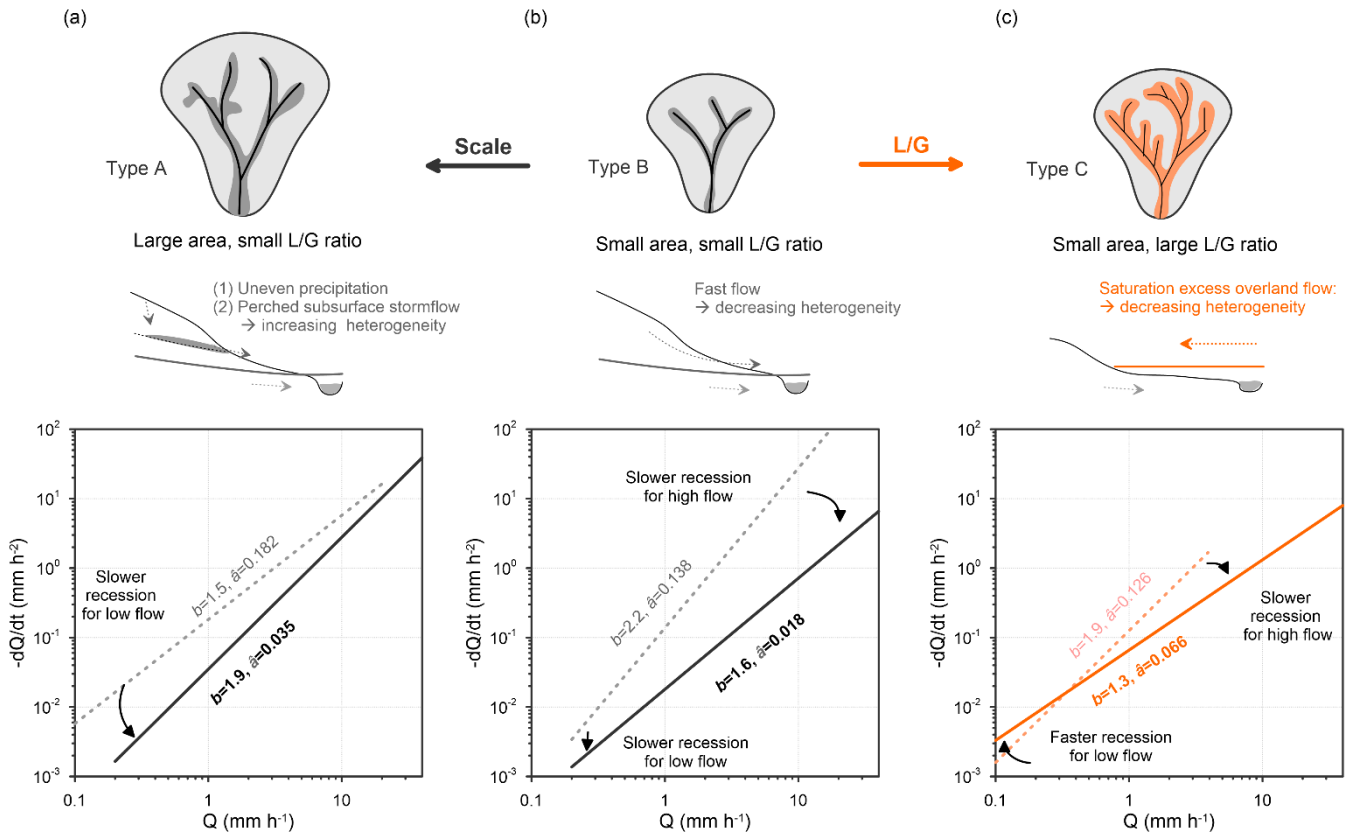
Figure 9: A conceptual diagram illustrating how landscape variables regulate the recession direction during rainstorms. The top row presents the drainage area and the stream network of three landscape types of catchments corresponding to Fig. 6b. The middle row presents the cross-sectional valley with descriptions of drainage behavior. Here, (a) type A, large catchment and steep slope, drains water via multiple sources of subsurface flow; (b) type B, small catchment and steep slope, drains water via fewer sources of subsurface flow; and (c) type C, small catchment and gentle slope, drains via the extension of the saturated zone along the riparian zone. Correspondingly, the bottom row shows how their recession parameters (or regressive line) in recession plots would move from light (dashed line) to heavy (solid line) rainstorms.